MODELING OF PIEZO STACK ACTUATORS AND THEIR APPLICATION IN ACTIVE VIBRATION CONTROL

Rupal Singhvi* and C. Venkatesan**

Abstract

This paper presents the vibration control of a highly simplified two degree of freedom model of a helicopter. The vibration control study has been performed using both active and passive vibration control schemes. In the case of active vibration control, the feedback mechanism affects the stiffness of the system; whereas in passive vibration control, the absorber mass affects the inertia of the system. The active control is achieved using a combination of piezo stack sensor and actuator mechanism. A finite element model for the piezo stack mechanism has been developed to obtain a relation between deformation, applied/induced potential and externally applied mechanical load. The results of this study indicate that inclusion of sensor and actuator units increases the natural frequency of the system due to increase in stiffness of the system. It is observed that in the case of active vibration control, the frequency response of acceleration of the system is highly sensitive to small variations in the magnitude of gain around its optimum value and insensitive to changes in excitation frequency; whereas in passive vibration control, the frequency response does not exhibit any significant change in the characteristics with respect to the variation in the absorber mass, while it is highly sensitive to changes in operating frequency.

Nomenclature

a_1, b_1, c_1, c_2 = constants
$\tilde{a}$, $\tilde{b}$ = vibration absorber dimensions
acc.ratio a_1= non-dimensional acceleration of hub
acc.ratio a_2= non-dimensional acceleration of fuselage
A = area
c = stiffness coefficients
C = damping coefficient
C_{ref} = reference damping coefficient
D = electric displacement
dV = elemental volume
e = piezoelectric coupling coefficient
E = electric field
$\tilde{E}$ = Young's modulus for metal layer
F = force
F_S, F_A = forces transmitted to hub and fuselage
F_{PS},F_{PA} = forces applied on the sensor/actuator
G = gain
$\overline{G}$ = magnitude of gain
K = stiffness
K_M, K_P = local stiffness matrix of metal and piezo respectively
L_M, L_P = length of metal and piezo layer respectively
L = total length of piezo stack
$\overline{L}$ = non-dimensional length ratio
M_H, M_F = mass of gear box/hub and fuselage respectively
N = Lagrangian shape function
$\overline{T}$ = traction
u = axial deflection
u_{tip} = tip deflection
V_{PA} = actuation voltage
X_1, X_2 = deflection of hub and fuselage respectively

Greek Symbols

ε = strain
η = phase angle
γ = shear strain
μ , μ_1, μ_2 = mass ratios
ω = frequency in rad/s
ω_{ref} = reference frequency
φ = angle in actuator/sensor mechanism

* Graduate Student ** Professor
Department of Aerospace Engineering, Indian Institute of Technology Kanpur, Kanpur-208 016, India; Email : cven@iitk.ac.in
Manuscript received on 07 Dec 2004; Paper reviewed, revised and accepted on 11 May 2005

Φ = electric potential
$\Phi_{induced}$ = induced potential
σ = stress
$\in$ = electric permittivity
ξ = damping ratio

Introduction

It is well known that helicopters are plagued with vibrations. The adverse effects of the vibratory loads increase with forward speed of the helicopter and also the cumulative fatigue damage to the structure increases with higher utilization of the vehicle. As a result, the vibratory loads restrict the operation and efficiency of the vehicle. The demand for increasing helicopter usage for passenger transportation and the demand for high-speed maneuverability helicopters for defense have underlined the need for vibration reduction. Vibration reduction can be achieved in a number of ways. Vibration reduction schemes adopted in helicopters can be classified as either *passive or active control methodologies* [1]. The passive control scheme includes hub or blade-mounted pendulum absorbers, anti resonant vibration isolation devices like dynamic anti resonant vibration isolator (DAVI), anti resonant isolation system (ARIS), and liquid inertia vibration eliminator (LIVE); structural modifications; and structural optimization. Active control methodologies include higher harmonic control (HHC), individual blade control (IBC), active flap control (AFC), and active control of structural response (ACSR). It may be noted that while HHC, IBC, and AFC control schemes are aimed at reducing the blade loads in the rotating frame, ACSR is employed in the non rotating frame to nullify the effect of vibratory hub loads on the fuselage.

The concept of an ACSR scheme is based on the principle of superposition of two independent responses of a linear system, such that the total response is zero [2]. The rotor loads are transmitted to fuselage through a gearbox support structure. The support structure is idealized as a spring, a damper, and a control force generator. In the passive vibration reduction scheme adopted in ARIS, the control force generator corresponds to a vibration absorber mass M_I as shown in Fig.1 (Refs. [3]- [5]). In Fig.1, M_F and M_H are the fuselage and hub masses respectively, and $F(t)$ represents the external excitation load. The motion of absorber mass is a function of the relative motion of the masses M_F and M_H. By suitably tuning the absorber mass (M_I), the relative hinge locations (L_1) and the overhang length (L_2), the vibratory level of fuselage mass M_F can be reduced, for a specific excitation frequency of $F(t)$. This scheme of vibration reduction has been successfully implemented in several operational helicopters in the world. In the active vibration control scheme of ACSR, the absorber mass is replaced by a control force generator which can be an electro hydraulic actuator or an electro mechanical actuator or a smart piezo actuator [6]-[9]. A schematic of the ACSR scheme having a combination of sensor and actuator pair is shown in Fig.2. In this study on active vibration control scheme, the sensor and the actuator are assumed to be made of piezo stacks. In the sensor mode, the piezo stacks develop an induced potential due to an applied external axial load (axial deformation). Whereas in the actuation mode, the applied external potential to the piezo stacks develops a deformation and the required control force. The closed

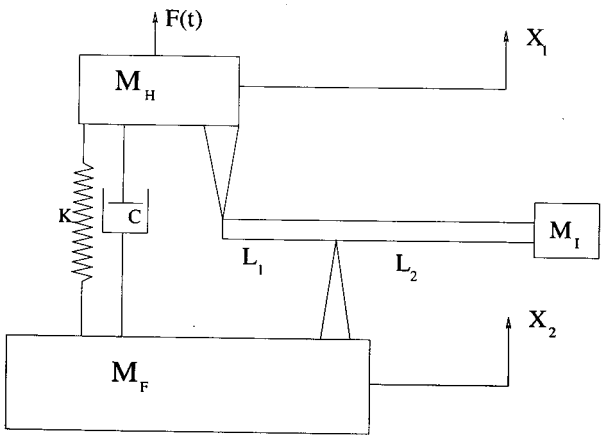

Fig.1 Rotor hub/fuselage dynamical model with ARIS type passive control

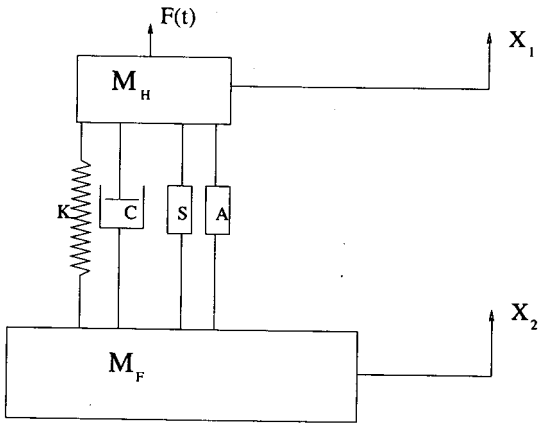

S – Sensor
A – Actuator

Fig.2 Rotor hub/fuselage dynamical model with ACSR type active control

loop (position feedback) scheme of vibration control is depicted in Fig.3. The objectives of this study are:-

- Formulation of a finite element model of a piezo stack actuator (or sensor) to obtain a linear relation between axial deformation, external axial load and applied (or induced) potential.
- Formulation of a closed loop active vibration control scheme (ACSR type) using a piezo sensor and actuator pair in a two degree of freedom system representing a highly simplified model of a helicopter.
- Analyze the frequency response behavior of the two degrees of freedom system under active control scheme and
- Compare the ACSR scheme of active vibration control with the ARIS scheme of passive vibration control. The reason for choosing these two control schemes is that in both cases the control force is proportional to the relative displacement between the hub and fuselage masses. However, in active vibration control scheme, the control force influences the stiffness of the system and in passive control scheme, the absorber mass influences the inertia of the system.

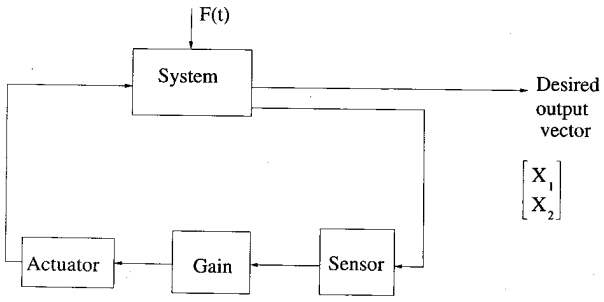

Fig.3 Closed loop position feedback control

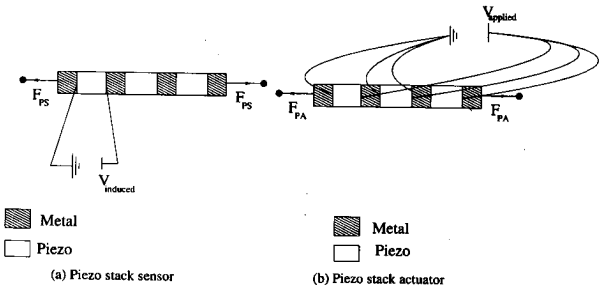

Fig.4 Piezo stack sensor and actuator (a) Piezo stack sensor (b) Piezo stack actuator

Modeling of Smart Piezo Stack Actuator/Sensor

The smart actuator is assumed to be a circular bar which consists of stacks of alternate layers of metal and piezoelectric material. The piezo stack actuator acts like a sensor when an induced potential is generated due to deformation caused by the external load. In the actuator mode, an external potential is applied across the piezo patches to develop deformation and force at the two ends of the actuator. Fig.4(a) shows the piezo stacks in sensor mode and Fig.4(b) shows the actuator mode. F_{PS} denotes the external axial force in the sensor mode and F_{PA} indicates the net force generated by the actuator due to an applied potential. In this section a finite element formulation is developed to obtain a relation between deformation, electric potential and external load acting at the ends of the smart actuator.

The general linear electro-elastic constitutive relation between stress, strain, electric field and electric displacement are given as [10].

$$\sigma_{ij} = c_{ijkl} \in_{kl} - e_{ijk} E_k \tag{1}$$

$$D_i = e_{ijk} \in_{jk} + \varepsilon_{ij} E_j \tag{2}$$

For piezoelectric materials, in the direction perpendicular to the poling direction the material is transversely isotropic. The elastic, piezoelectric and dielectric property matrices for PZT-5H material are given as follows [11].

$$c = \begin{bmatrix} c_{11} & c_{12} & c_{13} & 0 & 0 & 0 \\ c_{12} & c_{11} & c_{13} & 0 & 0 & 0 \\ c_{13} & c_{13} & c_{33} & 0 & 0 & 0 \\ 0 & 0 & 0 & c_{44} & 0 & 0 \\ 0 & 0 & 0 & 0 & c_{44} & 0 \\ 0 & 0 & 0 & 0 & 0 & c_{66} \end{bmatrix}$$

$$e = \begin{bmatrix} 0 & 0 & -e_{31} \\ 0 & 0 & -e_{31} \\ 0 & 0 & -e_{33} \\ 0 & -e_{15} & 0 \\ -e_{15} & 0 & 0 \\ 0 & 0 & 0 \end{bmatrix} \qquad \varepsilon = \begin{bmatrix} \varepsilon_1 & 0 & 0 \\ 0 & \varepsilon_1 & 0 \\ 0 & 0 & \varepsilon_3 \end{bmatrix}$$

The subscripts 1,2,3,4,5, and 6 refer to x, y, z, yz, xz, and xy respectively. The direction of poling is along z direction. The properties of the material PZT -5H are given in Table-1.

Figure 5 shows a piezo stack model acted upon by an external axial load. The direction of polarization in the piezo layer is along positive z direction which is along the longitudinal direction of the piezo stack. The thickness of metal and piezo layers are L_M and L_P respectively and the total length of the piezo stack is L. While formulating the finite element model for the piezo stack, several assumptions have been made which are given as follows:

- Piezoelectric material is transversely isotropic.
- The cylindrical surface of the piezo stack are stress free. Therefore, the stress σ_x and σ_y are zero throughout the specimen.
- Shear strains $\gamma_{yz} = \gamma_{xy} = \gamma_{zx} = 0$ and shear stresses are assumed to be zero.
- Electric field acts only in z-direction i.e. $E_x = E_y = 0$.
- The metal and piezo layers respectively are assumed to have uniform thickness through out the stack.
- The inertia and damping effects of piezo stack are not considered.

Finite Element Formulation

The finite element formulation is based on the application of variational principle. The variational form of the linear electro-elastic problem is given as [12].

$$\int_v \sigma_{ij}\, \delta \in_{ij} dV - \int_v D_i\, \delta E_i\, dV = \int_s \overline{T}_i\, \delta u_i\, dS$$

Noting that only σ_z and E_z exist in the piezo layer, and there is no traction force, the variational formulation for the piezo layer can be written as

$$\int_v \sigma_z\, \delta \in_z dV - \int_v D_z\, \delta E_z\, dV = 0 \qquad (3)$$

Based on the assumptions made in the formulation, the constitutive equations can be reduced as [12] and [13],

Table-1 : Material properties for PZT-5H

GPa					
c_{11}	c_{12}	c_{13}	c_{33}	c_{44}	c_{66}
138.33	93.16	95.06	131.26	21.05	21.05
C/m^2					
e_{31}		e_{33}		e_{15}	
-4.0329		16.5815		12.29	
F/m					
ε_1		ε_3			
15293 x 10^{-12}		15028 x 10^{-12}			

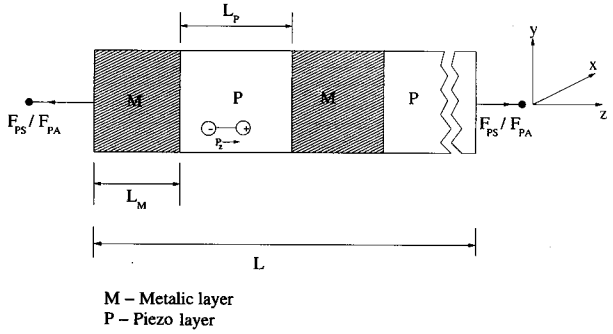

Fig.5 Piezo stack model

$$\sigma_z = -e^* E_z + c^* \in_z \qquad (4)$$

$$D_z = \varepsilon^* E_z + e^* \in_z \qquad (5)$$

Where,

$$c^* = c_{33} - \frac{2c_{13}^2}{c_{11} + c_{12}}$$

$$e^* = \frac{2c_{13}\, e_{31}}{c_{11} + c_{12}} - e_{33}$$

$$\varepsilon^* = \varepsilon_3 + \frac{2e_{31}^2}{c_{11} + c_{12}}$$

Substituting equations (4) and (5) in equation (3) yields

$$\int_v (c^* \in_z - e^* E_z)\, \delta \in_z dV - \int_v (\varepsilon^* E_z - e^* \in_z)\, \delta E_z\, dV = 0 \qquad (6)$$

Substituting for $\in_z = \frac{\partial u}{\partial z}$ and $E_z = -\frac{\partial \Phi}{\partial z}$, equation (6) can be written as,

$$\int_0 \left(c^* \frac{\partial u}{\partial z} + e^* \frac{\partial \Phi}{\partial z} \right) \frac{\partial\, \delta u}{\partial z}\, dV + \int_v (-\varepsilon^* \frac{\partial \Phi}{\partial z} + e^* \frac{\partial u}{\partial z}) \frac{\partial\, \delta \Phi}{\partial z}\, dV = 0$$

Integrating over the cross-sectional area, one obtains

$$A \int_0^{L_P} \left(c^* \frac{\partial u}{\partial z} + e^* \frac{\partial \Phi}{\partial z} \right) \frac{\partial\, \delta u}{\partial z}\, dz + A \int_0^{L_p} (-\varepsilon^* \frac{\partial \Phi}{\partial z} + e^* \frac{\partial u}{\partial z}) \frac{\partial\, \delta \Phi}{\partial z}\, dz = 0 \qquad (7)$$

The finite element formulation satisfies the displacement continuity at the interface between piezo and metallic layers. Both axial displacement u and electric potential Φ are assumed to be quadratic functions of z. Fig.6 shows the nodal degrees of freedom in the metallic and the piezo layers. The element used for modeling the piezo patch has three nodes. Each node has two degrees of freedom. These correspond to one extensional displacement in z-direction and one electric potential. This results in a stiffness matrix of the order of 6*6 for the piezo patch element. Whereas the element for the metallic layer has three nodes, having one degree of freedom per node. These correspond to extensional degree of freedom in the z direction. The stiffness matrix is of the order of 3*3 for the metallic layer (Fig. 6).

The axial displacement and electric potential are given in the discretized form as

$$u(z) = \sum_{j=1}^{3} u_j N_j \qquad \delta u_i = \delta u_i N_i$$

$$\Phi(z) = \sum_{j=1}^{3} \Phi_j N_j \qquad \delta \Phi_i = \delta \Phi_i N_i$$

where u_j and Φ_j are the nodal degrees of freedom and N_j are quadratic Lagrangian shape functions, which are given as,

$$N_1 = \left(1 - \frac{z}{L_P}\right)\left(1 - \frac{2z}{L_P}\right)$$

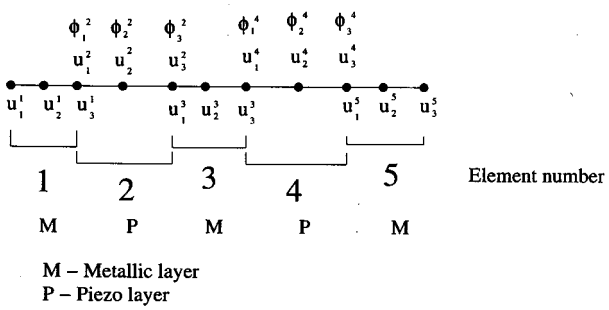

Fig.6 Finite element model of piezo stack actuator

$$N_2 = \left(\frac{4z}{L_P}\right)\left(1 - \frac{z}{L_P}\right)$$

$$N_3 = \left(-\frac{z}{L_P}\right)\left(1 - \frac{2z}{L_P}\right)$$

Substituting for u and Φ in equation (7), the virtual work formulation can be written as

$$\sum_{i=1}^{3}\sum_{j=1}^{3} \left\{ A \int_0^{L_p} \left(c^* u_j \frac{\partial N_j}{\partial z} + e^* \Phi_j \frac{\partial N_j}{\partial z} \right) \frac{\partial N_i}{\partial z} \delta u_i\, dz + A \int_0^{L_p} (-\varepsilon^* \Phi_j \frac{\partial N_j}{\partial z} + e^* u_j \frac{\partial N_j}{\partial z}) \frac{\partial N_i}{\partial z} \delta \Phi_i\, dz \right\} = 0 \qquad (8)$$

On substituting for u, Φ, δu, and $\delta\Phi$ in equation (8), the local stiffness matrix for the piezo layer can be obtained as,

$$K_P = \frac{A}{L_P} \begin{bmatrix} \frac{7c^*}{3} & \frac{-8c^*}{3} & \frac{c^*}{3} & \frac{7e^*}{3} & \frac{-8e^*}{3} & \frac{e^*}{3} \\ \frac{-8c^*}{3} & \frac{16c^*}{3} & \frac{-8c^*}{3} & \frac{-8e^*}{3} & \frac{16e^*}{3} & \frac{-8e^*}{3} \\ \frac{c^*}{3} & \frac{-8c^*}{3} & \frac{7c^*}{3} & \frac{e^*}{3} & \frac{-8e^*}{3} & \frac{7e^*}{3} \\ \frac{7e^*}{3} & \frac{-8e^*}{3} & \frac{e^*}{3} & \frac{-7\varepsilon^*}{3} & \frac{8\varepsilon^*}{3} & \frac{-\varepsilon^*}{3} \\ \frac{-8e^*}{3} & \frac{16e^*}{3} & \frac{-8e^*}{3} & \frac{-8\varepsilon^*}{3} & \frac{-16\varepsilon^*}{3} & \frac{8\varepsilon^*}{3} \\ \frac{e^*}{3} & \frac{-8e^*}{3} & \frac{7e^*}{3} & \frac{-\varepsilon^*}{3} & \frac{8\varepsilon^*}{3} & \frac{-7\varepsilon^*}{3} \end{bmatrix}$$

The nodal displacement vector is $\begin{bmatrix} u_1 \\ u_2 \\ u_3 \\ \Phi_1 \\ \Phi_2 \\ \Phi_3 \end{bmatrix}$

The element stiffness matrix for a metallic layer can be written as [14]

$$K_M = \frac{\tilde{E}\,A}{3L_M}\begin{bmatrix} 7 & -8 & 1 \\ -8 & 16 & -8 \\ 1 & -8 & 7 \end{bmatrix}$$

where $\tilde{E}$ is the Young's Modulus of Elasticity.

The nodal displacement vector in this case is given as

$$\begin{bmatrix} u_1 \\ u_2 \\ u_3 \end{bmatrix}$$

After imposing the displacement continuity and the boundary conditions, the global discretized linear electro-elastic equilibrium equation for the entire piezo stack actuator can be written as,

$$[K]\{a\} = \{F\} \tag{9}$$

where $[K]$ is the global stiffness matrix, $\{a\}$ is vector of global degrees of freedom, and $\{F\}$ is the global load vector.

Piezo Stack Under Sensing Mode

Assume that the piezo stack is used as a sensing element and is acted on by an external axial load F_{PS} as shown in Fig.4(a). One end of the piezo layer is grounded and the induced potential across the piezo layer is measured at the other end of the piezo layer. Using equation (9), the relation between the tip deflection and potential induced as a function of the load F_{PS} can be expressed as

$$u_{tip} = a_1 F_{PS} \tag{10}$$

$$\Phi_{induced} = b_1 F_{PS} \tag{11}$$

Table-2 : Data for modeling the piezo stack sensor/actuator

Diameter of the piezo stack	=	2 mm
Total length of the piezo stack	=	101 mm
Number of layers	=	101 (alternate MPM..M)
Thickness of the metal layer	=	0.5 mm
Thickness of the piezo layer	=	1.5 mm
Young's modulus for metal (Aluminium) $\tilde{E}$	=	70 GPa
Geometric data for mechanism :		
$\tilde{a}$	=	58.74 mm
$\tilde{b}$	=	101 mm

where a_1 and b_1 are constants which are evaluated from the finite element analysis. It may be noted that the external mechanical load F_{PS} is considered positive when tensile and negative when it is compressive. Since both u_{tip} and Φ are linear functions of the applied force, the constants a_1 and b_1 are obtained by applying a unit force at the ends of the piezo stack sensor i.e., $F_{PS} = 1N$. For a piezo stack having a diameter of 2mm, and a total length of 101mm the values of a_1 and b_1 are found to be (other relevant data are given in Tables-1 and 2)
$a_1 = 4.18031 * 10^{-7}\ m/N$ and $b_1 = 7.8955\ V/N$.

Piezo Stack Under Actuation Mode

In actuation mode, the piezo stack is acted upon by external axial load F_{PA} (F_{PA} is taken to be positive when tensile and negative when it is compressive) and an external potential across the piezo layers as shown in Fig.4(b). The tip deflection as a function of external axial load F_{PA} and actuation voltage V_{PA} can be expressed as,

$$u_{tip} = c_1 F_{PA} + c_2 V_{PA} \tag{12}$$

where $c_1$and c_2 are constants evaluated from the finite element formulation given in equation (9). The constant c_1 is obtained by applying a unit force and zero voltage ($F_{PA} = 1N$ and $V_{PA} = 0V$) and the constant c_2 is obtained using $F_{PA} = 0N$ and $V_{PA} = 1V$. For the data given in Tables-1 and 2, the values of c_1 and c_2 are found to be
$c_1 = 5.65686 * 10^{-7}\ m/N$ and $c_2 = -1.87 * 10^{-8}\ m/V$

Note that the value of the constant c_2 is negative indicating that for a positive voltage the piezo stack actuator will undergo a compression. The reason for this behavior is due to the assumption that the polarization vector in the piezo layer is along the positive z direction and the electric field is along the negative z direction. Equation (12) can be used to calculate the block force required to have zero tip deflection under the action of any external actuation voltage.

Piezo Stack Mechanism for Sensor/Actuator

In order to amplify the deformation of the piezo stack, a simple mechanism as shown in Fig.7 is used. The members AB, AD, CB, and CD are assumed to be rigid axial members. All the joints are assumed to be frictionless hinges. The piezo stack actuator is connected between the nodes B and D. In both sensing and actuation modes, this mechanism is incorporated in the vibration control problem as shown in Fig.2. The point A is attached to the mass M_H and point C is attached to mass M_F. From the un-deformed and the deformed configurations of the piezo stack mechanism, the relation between the axial deformation of the piezo stack (u_{tip}) and the relative displacement between hub and fuselage (X_1 - X_2), can be written as,

$$u_{tip} = -\frac{\sqrt{4\tilde{a}^2 - \tilde{b}^2}}{\tilde{b}}(X_1 - X_2) \tag{13}$$

The relation between the force F_S (transmitted to the hub and fuselage by the sensor mechanism) and the external axial load on the sensor F_{PS} is given as

$$F = F_{PS} \tan \Psi \tag{14}$$

where $\tan \Psi = \dfrac{\sqrt{4\tilde{a}^2 - \tilde{b}^2}}{\tilde{b}}$

Similarly the relation between the force F_A (transmitted to the hub and fuselage by the actuator mechanism) and the external axial load on the actuator F_{PA} is given as

$$F_A = F_{PA} \tan \Psi \tag{15}$$

In deriving these relations, it is assumed that the sensor and actuator mechanisms undergo small deformation.

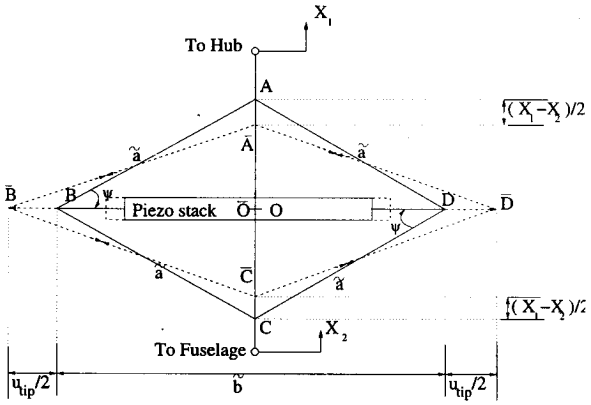

$u_{tip} = -\frac{\sqrt{4\tilde{a}^2 - \tilde{b}^2}}{\tilde{b}}(X_1 - X_2)$

(a) Deformation configuration

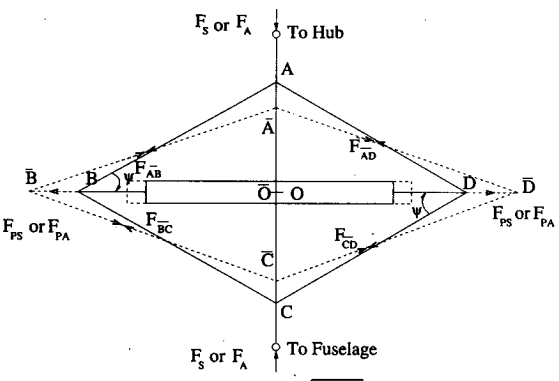

$F_S = F_{PS} \tan \Psi; \tan \Psi = \frac{\sqrt{4\tilde{a}^2 - \tilde{b}^2}}{\tilde{b}}$

(b) Force balance

Fig.7 Piezo stack mechanism before and after deformation (a) Deformation configuration, (b) Force balance

Sensor Mechanism

Substituting equations (13) and (14) in equations (10) and (11), the relations between sensor force F_S, induced potential $\Phi_{induced}$ and the relative displacement (X_1 - X_2) can be respectively written as

$$F_S = -\frac{\sqrt{4\tilde{a}^2 - \tilde{b}^2}}{a_1 \tilde{b}} \tan\Psi\,(X_1 - X_2) = -F^*\,(X_1 - X_2) \tag{16}$$

$$\Phi_{induced} = \frac{b_1 F_S}{\tan \Psi} = --\frac{\sqrt{4\tilde{a}^2 - \tilde{b}^2}}{a_1 \tilde{b}} b_1 (X_1 - X_2) \tag{17}$$

Substituting the geometric data of the mechanism given in Table-2, the value of F* is found to be F* = 8.44 x 10^5 *N/m*.

Actuator Mechanism

Substituting equations (13) and (15) in equation (12), the relations between actuator force F_A, actuation potential V_{PA} and the relative displacement (X_1 - X_2) can be written as

$$-\frac{\sqrt{4\tilde{a}^2-\tilde{b}^2}}{\tilde{b}}(X_1-X_2)=c_1\frac{F_A}{\tan\Psi}+c_2\,V_{PA} \tag{18}$$

For closed loop vibration control, the actuation potential is related to the induced potential in the sensor through gain which is given as $V_{PA} = G\,\Phi_{induced}$. Rearranging the terms in equation (18), the actuator force can be expressed as

$$F_A=-\frac{\sqrt{4\tilde{a}^2-\tilde{b}^2}}{\tilde{b}c_1}\tan\Psi\,(X_1-X_2)-\frac{c_2}{c_1}\tan\Psi\,G\,\Phi_{induced} \tag{19}$$

Substituting equation (17) in equation (19) it can be seen that,

$$F_A=-\bar{F}\,(X_1-X_2) \tag{20}$$

For the data given in Table-2, the value of $\bar{F}$ is found to be $\bar{F}$ = 6.238 x 10^5+2.2 x 10^5G. It may be noted that the closed loop feedback gain can be given as

$$G=\bar{G}e^{i\eta} \tag{21}$$

where $\bar{G}$ is magnitude and η is the phase.

Analysis of Vibration Control Problem

A simplified two degrees of freedom model shown in Fig.2 is analyzed for vibration control problems. The external excitation force acting on the mass M_H is assumed to be of the form $F(t) = F_0e^{i\omega t}$, where ω is the excitation frequency. The vibration analysis has been carried out for two cases; namely (i) in addition to spring and damper, only a sensor is provided between hub and fuselage, and (ii) in addition to spring and damper, both sensor and actuator are incorporated between hub and fuselage.

Vibration Analysis with Sensor Only

The equation of motion of the system, when only sensor is attached between the hub and fuselage, can be written as

$$M_H\ddot{X}_1+C\,(\dot{X}_1-\dot{X}_2)+K\,(X_1-X_2)=F_S+F_0e^{i\omega t}$$

$$M_F\ddot{X}_2+C\,(\dot{X}_2-\dot{X}_1)+K\,(X_2-X_1)=-F_S$$

Substituting for F_S, from equation (16), one obtains

$$M_H\ddot{X}_1+C\,(\dot{X}_1-\dot{X}_2)+K\,(X_1-X_2)+F^*\,(X_1-X_2)=F_0e^{i\omega t}$$

$$M_F\ddot{X}_2+C\,(\dot{X}_2-\dot{X}_1)+K\,(X_2-X_1)+F^*\,(X_2-X_1)=0$$

Assuming a solution of the form $X_1=\bar{X}_1e^{i\omega t}$ and $X_2=\bar{X}_2e^{i\omega t}$, the frequency response of non dimensional displacement can be written as,

$$\frac{\bar{X}_1}{F_0/K}=\frac{1+\frac{F^*}{K}-\left(\frac{\omega}{\omega_{ref}}\right)^2+i\frac{2\xi\omega}{\omega_{ref}}}{\mu\left(\frac{\omega}{\omega_{ref}}\right)^4-\left(1+\frac{F^*}{K}\right)(1+\mu)\left(\frac{\omega}{\omega_{ref}}\right)^2-i2\xi\left(\frac{\omega}{\omega_{ref}}\right)^3(1+\mu)} \tag{22}$$

and

$$\frac{\bar{X}_2}{F_0/K}=\frac{1+\frac{F^*}{K}+i\frac{2\xi\omega}{\omega_{ref}}}{\mu\left(\frac{\omega}{\omega_{ref}}\right)^4-\left(1+\frac{F^*}{K}\right)(1+\mu)\left(\frac{\omega}{\omega_{ref}}\right)^2-i2\xi\left(\frac{\omega}{\omega_{ref}}\right)^3(1+\mu)} \tag{23}$$

where,

$$\mu=\frac{M_H}{M_F}=Mass\ ratio$$

$$\omega_{ref}^2=\frac{K}{M_f}=Reference\ frequency$$

$$C=Damping\ coefficient$$

$$C_{ref}=2M_F\,\omega_{ref}=Reference\ damping\ coefficient$$

$$\xi=\frac{C}{C_{ref}}=Damping\ ratio$$

The frequency response of non dimensional acceleration of the masses M_H and M_F can be respectively written as,

acc. ratio a_1

$$= \frac{1 + \frac{F^*}{K} - (\frac{\omega}{\omega_{ref}})^2 + i\frac{2\xi\omega}{\omega_{ref}}}{\mu(\frac{\omega}{\omega_{ref}})^2 - (1 + \frac{F^*}{K})(1+\mu) - i2\xi(\frac{\omega}{\omega_{ref}})(1+\mu)}$$

acc. ratio a_2

$$= \frac{1 + \frac{F^*}{K} + i\frac{2\xi\omega}{\omega_{ref}}}{\mu(\frac{\omega}{\omega_{ref}})^2 - (1 + \frac{F^*}{K})(1+\mu) - i2\xi(\frac{\omega}{\omega_{ref}})(1+\mu)}$$

Vibration Analysis with Sensor and Actuator

The equations of motion of the system having both a sensor and actuator, as shown in Fig.2 can be written as,

$$M_H\ddot{X}_1 + C(\dot{X}_1 - \dot{X}_2) + K(X_1 - X_2) = F_A + F_S + F_0 e^{i\omega t}$$

$$M_F\ddot{X}_2 + C(\dot{X}_2 - \dot{X}_1) + K(X_2 - X_1) = -(F_A + F_S)$$

Substituting for F_S and F_A from equations (16) and (20), one obtains

$$M_H\ddot{X}_1 + C(\dot{X}_1 - \dot{X}_2) + K(X_1 - X_2) + \tilde{F}(X_1 - X_2) = F_0 e^{i\omega t}$$

$$M_F\ddot{X}_2 + C(\dot{X}_2 - \dot{X}_1) + K(X_2 - X_1) + \tilde{F}(X_2 - X_1) = 0$$

It may be noted that $\tilde{F} = \bar{F} + F^*$ which is equal to $\tilde{F} = 14.678 \times 10^5 + 2.2 \times 10^5 \bar{G} e^{in}$.

Assuming $X_1 = \bar{X}_1 e^{i\omega t}$ and $X_2 = \bar{X}_2 e^{i\omega t}$, the frequency response of non dimensional displacement can be written as,

$$\frac{\bar{X}_1}{F_0/K} = \frac{1 + \frac{\tilde{F}}{K} - (\frac{\omega}{\omega_{ref}})^2 + i\frac{2\xi\omega}{\omega_{ref}}}{\mu(\frac{\omega}{\omega_{ref}})^4 - (1 + \frac{\tilde{F}}{K})(1+\mu)(\frac{\omega}{\omega_{ref}})^2 - i2\xi(\frac{\omega}{\omega_{ref}})^3(1+\mu)} \quad (24)$$

$$\frac{\bar{X}_2}{F_0/K} = \frac{1 + \frac{\tilde{F}}{K} + i\frac{2\xi\omega}{\omega_{ref}}}{\mu(\frac{\omega}{\omega_{ref}})^4 - (1 + \frac{\tilde{F}}{K})(1+\mu)(\frac{\omega}{\omega_{ref}})^2 - i2\xi(\frac{\omega}{\omega_{ref}})^3(1+\mu)} \quad (25)$$

The magnitudes of system response can be obtained for various values of gain $\bar{G}$ and phase η.

The frequency response of non dimensional acceleration of the masses M_H and M_F can be respectively written as,

acc. ratio a_1

$$= \frac{1 + \frac{\tilde{F}}{K} - (\frac{\omega}{\omega_{ref}})^2 + i\frac{2\xi\omega}{\omega_{ref}}}{\mu(\frac{\omega}{\omega_{ref}})^2 - (1 + \frac{\tilde{F}}{K})(1+\mu) - i2\xi(\frac{\omega}{\omega_{ref}})(1+\mu)}$$

acc. ratio a_2

$$= \frac{1 + \frac{\tilde{F}}{K} + i\frac{2\xi\omega}{\omega_{ref}}}{\mu(\frac{\omega}{\omega_{ref}})^2 - (1 + \frac{\tilde{F}}{K})(1+\mu) - i2\xi(\frac{\omega}{\omega_{ref}})(1+\mu)}$$

Frequency Response of Passive Vibration Control System with ARIS (Fig.1)

For the sake of comparison, the frequency response of a passive vibration control system shown in Fig.1 is also analyzed. The equations of motion of the system (taken from Ref. [5]) can be written as,

$$M_H\ddot{X}_1 + M_I\left(\frac{L_2}{L_1}\right)^2\ddot{X}_1 - M_I\frac{L_2(L_1+L_2)}{L_1^2}\ddot{X}_2 + C(\dot{X}_1 - \dot{X}_2) + K(X_1 - X_2) = F_0 e^{i\omega t} \quad (26)$$

$$M_F\ddot{X}_2 + M_I\left(\frac{L_1+L_2}{L_1}\right)^2\ddot{X}_2 - M_I\frac{L_2(L_1+L_2)}{L_1^2}\ddot{X}_1 + C(\dot{X}_2 - \dot{X}_1) + K(X_2 - X_1) = 0 \quad (27)$$

Based on these equations, the frequency response of non-dimensional displacement can be written as,

$$\frac{X_1}{F_0/K} = \left(\frac{\omega_{ref}}{\omega}\right)^2 \left[\frac{1 - \left(\frac{\omega}{\omega_{ref}}\right)^2 \left(1 + \mu_2 \left(1 + \bar{L}\right)^2\right) + i\,\frac{2\xi\omega}{\omega_{ref}}}{\left(\frac{\omega}{\omega_{ref}}\right)^2 \left(\mu_1 + \mu_2 \bar{L}^2 + \mu_1 \mu_2 \left(1 + \bar{L}\right)^2\right) - \left(1 + \mu_1 + \mu_2\right) - i2\xi \left(\frac{\omega}{\omega_{ref}}\right) \left(1 + \mu_1 + \mu_2\right)} \right]$$

$$\frac{X_2}{F_0/K} = \left(\frac{\omega_{ref}}{\omega}\right)^2 \left[\frac{1 - \left(\frac{\omega}{\omega_{ref}}\right)^2 \left(\mu_2 \bar{L} \left(1 + \bar{L}\right)\right) + i\,\frac{2\xi\omega}{\omega_{ref}}}{\left(\frac{\omega}{\omega_{ref}}\right)^2 \left(\mu_1 + \mu_2 \bar{L}^2 + \mu_1 \mu_2 \left(1 + \bar{L}\right)^2\right) - \left(1 + \mu_1 + \mu_2\right) - i2\xi \left(\frac{\omega}{\omega_{ref}}\right) \left(1 + \mu_1 + \mu_2\right)} \right]$$

where,

M_H, M_F, M_I - Hub, fuselage and isolator mass respectively

$$\mu_1 = \frac{M_H}{M_F}$$

$$\mu_2 = \frac{M_I}{M_F}$$

$$\bar{L} = \frac{L_2}{L_1}$$

The frequency response of non dimensional acceleration of the masses M_H and M_F can be respectively written as,

$$acc.\ ratio\ a_1 = \left[\frac{1 - \left(\frac{\omega}{\omega_{ref}}\right)^2 \left(1 + \mu_2 \left(1 + \bar{L}\right)^2\right) + i\,\frac{2\xi\omega}{\omega_{ref}}}{\left(\frac{\omega}{\omega_{ref}}\right)^2 \left(\mu_1 + \mu_2 \bar{L}^2 + \mu_1 \mu_2 \left(1 + \bar{L}\right)^2\right) - \left(1 + \mu_1 + \mu_2\right) - i2\xi \left(\frac{\omega}{\omega_{ref}}\right) \left(1 + \mu_1 + \mu_2\right)} \right]$$

$$acc.\ ratio\ a_2 = \left[\frac{1 - \left(\frac{\omega}{\omega_{ref}}\right)^2 \left(\mu_2 \bar{L} \left(1 + \bar{L}\right)\right) + i\,\frac{2\xi\omega}{\omega_{ref}}}{\left(\frac{\omega}{\omega_{ref}}\right)^2 \left(\mu_1 + \mu_2 \bar{L}^2 + \mu_1 \mu_2 \left(1 + \bar{L}\right)^2\right) - \left(1 + \mu_1 + \mu_2\right) - i2\xi \left(\frac{\omega}{\omega_{ref}}\right) \left(1 + \mu_1 + \mu_2\right)} \right]$$

Results and Discussion

Using the frequency response functions derived for various cases, several parametric studies have been performed to evaluate the influence of piezo actuator/sensor on the dynamic characteristics of the system. A comparative study is also made to bring out the essential difference between active control (incorporating ACSR scheme) and a passive control system (having ARIS scheme). Since this study is performed to understand the influence of piezo sensor/actuator on active vibration control scheme, no restriction has been imposed on induced and applied potential across the piezo layer. The data used for the dynamic analysis are given in Table-3. The reference frequency ω_{ref} for non dimensionalization is taken as 6.78Hz (42.61rad/s). The baseline system is taken as the system without any vibration control mechanism, which is excited by a force having a non-dimensional frequency 3.17.

Table-3 : Data for vibration control

Reference quantities :

M_b = 65 kg

R = 6 m

Ω = 32 rad/s

Data :

M_F = 2200 kg

M_H = 300 kg

$K = 60.01 \times M_b \times \Omega^2 = 4 \times 10^6$ N/m

$\omega_{ref} = \sqrt{\frac{K}{M_F}} = 42.61 \ rad/s$

$C_{ref} = 2 \times M_F \times \omega_{ref} = 1.87 \times 10^5$ Ns/m

$C = 0.033 \times M_b \times \Omega = 68.64$ Ns/m

$L = \frac{L_2}{L_1} = 12.5$

Magnitude of gain $\overline{G}$ = 0 - 60

Phase η = 0 -360 deg in steps of 90 deg

Figure 8 shows the frequency response of the displacement and acceleration of the system given in Fig.2. The frequency response is provided for three different cases: (a) baseline system without sensor and actuator, (b) system with sensor only, and (c) system with both sensor and actuator with gain $\overline{G}$ = 0. The frequency response curves show that the natural frequency of the system for case (a) is 2.89 (19.58 Hz). Inclusion of sensor shifts the natural frequency to 3.17 (21.55 Hz). Addition of sensor and actuator further shifts the natural frequency to 3.24 (22.89 Hz). The reason for the shift in natural frequency is due to increase in stiffness by the addition of piezo sensor and actuator units. The results indicate that the response of the masses at resonance frequency for all the cases are almost the same.

Keeping the non-dimensional excitation frequency of the forcing function $F(t)$ as 3.17, the displacement and acceleration response of closed loop vibration control of the system are evaluated for various values of gain G and the results are shown in Fig.9. The results have been generated for several magnitudes and phase angles of gain G. For the sake of conciseness, only those results pertaining to phase angle η = 0, 90, 180, 270, 360 deg. are presented. The pairs of figures under the cases (a), (b) and (c) show the variation of non-dimensional displacement and acceleration as a function of the magnitude of gain for fixed phase angle. The results show that for the phase angle η = 0 (or 360 deg.) and η = 90 deg. (or 270deg.), the displacement and acceleration response of the masses M_H and M_F decrease monotonically with increase in gain and reach a constant value asymptotically. Whereas, for the phase angle η = 180deg., the frequency response shows a minimum for the response of the fuselage mass M_F at a value of gain $\overline{G}$ = 24.8. A resonant peak is also observed for a gain of 2.8. From Fig.8a, it can be noted that the baseline acceleration response for masses M_H (acc. ratio a_1) and M_F (acc. ratio a_2) are 1.5784 and 0.62 respectively. It is interesting to note from Fig.9 that the magnitude of acceleration response of both the masses is well below the baseline response for all values of gains and phase angles (except near gain $\overline{G}$ = 2.8 for case η = 180deg.). This result clearly shows that the closed loop control system has sufficient gain and phase margins for vibration reduction of the system.

The frequency response of the closed loop vibration control system for three different gain values are shown in Fig.10. The phase angle of gain η is fixed at η = 180deg. The magnitude of the gain values are taken as $\overline{G}$ = 23, 24.8, and 25. The response curves show that as the gain is increased from 23 to 25, the natural frequency of the system shifts to a lower value. There is no resonant peak for the case when $\overline{G}$ = 25. Fig.10 also indicates that the nature of the closed loop system is observed to be highly sensitive to small variations in the magnitude of gain around the optimum value $\overline{G}$ = 24.8. It is observed that the natural frequency shifts drastically with a small variation in the magnitude of the gain. Combining the results shown in Fig.8c and Fig.10, it can be noted that the non-dimensional natural frequency shifts from 3.24 (for a system with both sensor and actuator ($\overline{G}$ = 0), Fig.8c) to 0.92 (for the same system with a gain value of $\overline{G}$ = 23, Fig.10a) and then to 0.11 (for a gain of $\overline{G}$ = 24.8, Fig.10b); and no resonant peak is observed for a gain of $\overline{G}$ = 25 and beyond. The asymptotic variation of the acceleration response for the three cases are shown in Fig.11. The asymptotic values of the acceleration response of masses M_H and M_F, for gain values of $\overline{G}$ = 23, 24.8, and 25 are 0.87, -1.68; 0.86, -3.02; and 0.86, -2.67 respectively. It is observed that the asymptotic value of the acceleration response of the mass M_F is a minimum ($\simeq$ -3) for a gain $\overline{G}$ = 24.8, and there is no significant variation in the acceleration response of M_H. It can be seen that, around the non-dimensional excitation frequency of 3.17, the variation in acceleration response of the system is negligible with respect to the frequency.

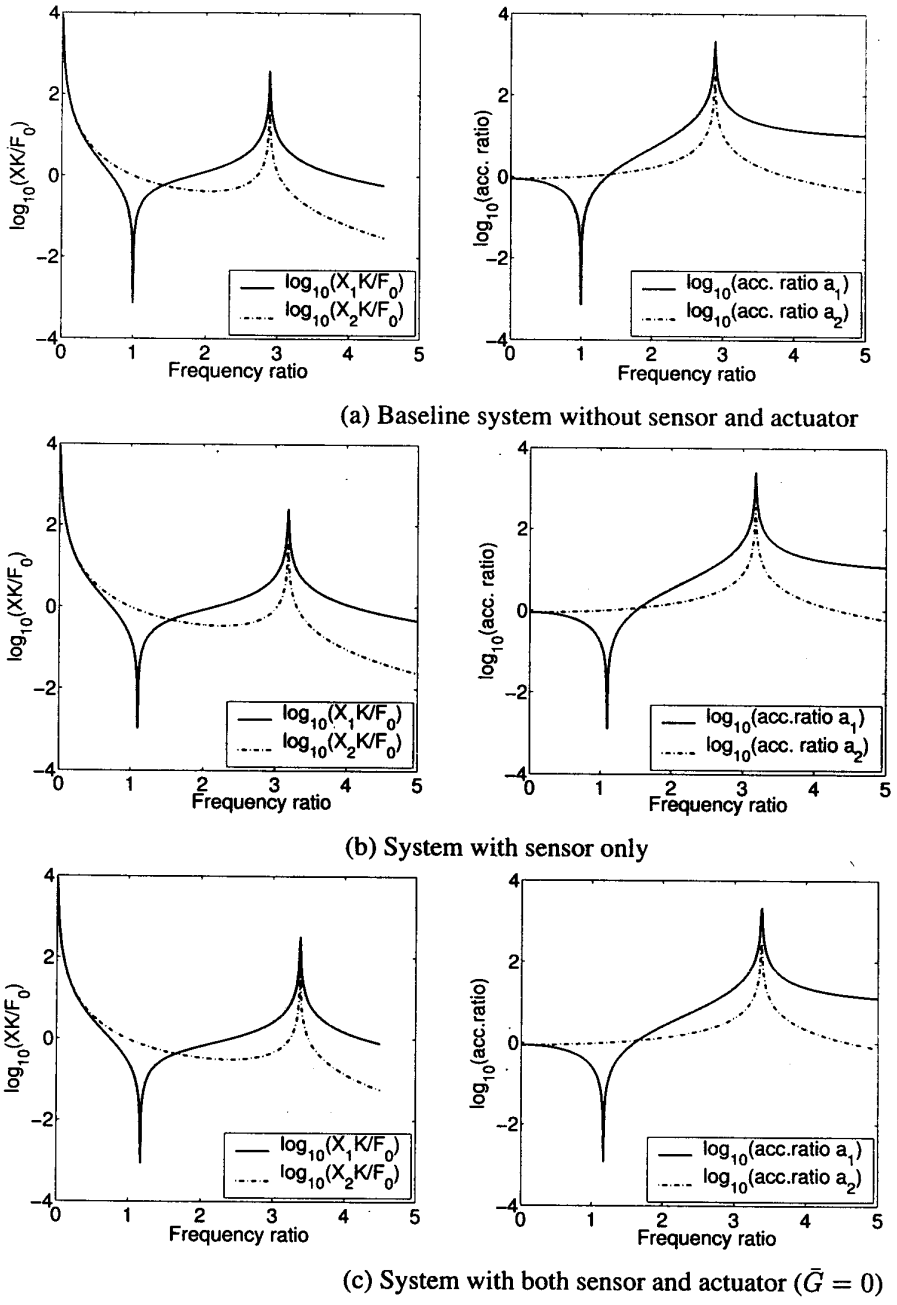

Fig.8 Frequency response of non dimensional displacement and acceleration with piezo stack sensor and actuator mechanism (a) Baseline system without sensor and actuator, (b) System with sensor only, (c) System with both sensor and actuator

The results corresponding to passive vibration control scheme, shown in Fig.1, are presented in Figs.12 and 13. The data used for this study are given in Table-3. Even in this case, the non-dimensional excitation frequency of the forcing function is fixed at 3.17. The influence of absorber mass on the system response is shown in Fig.12. The fuselage vibratory response is found to be a minimum when the absorber mass M_I = 1.3kg.

The frequency response of the passive vibration control system for three different values of absorber mass is shown in Fig.13. The values of the absorber mass are taken as M_I = 1.0 kg, 1.3 kg, and 1.5kg. The response curves

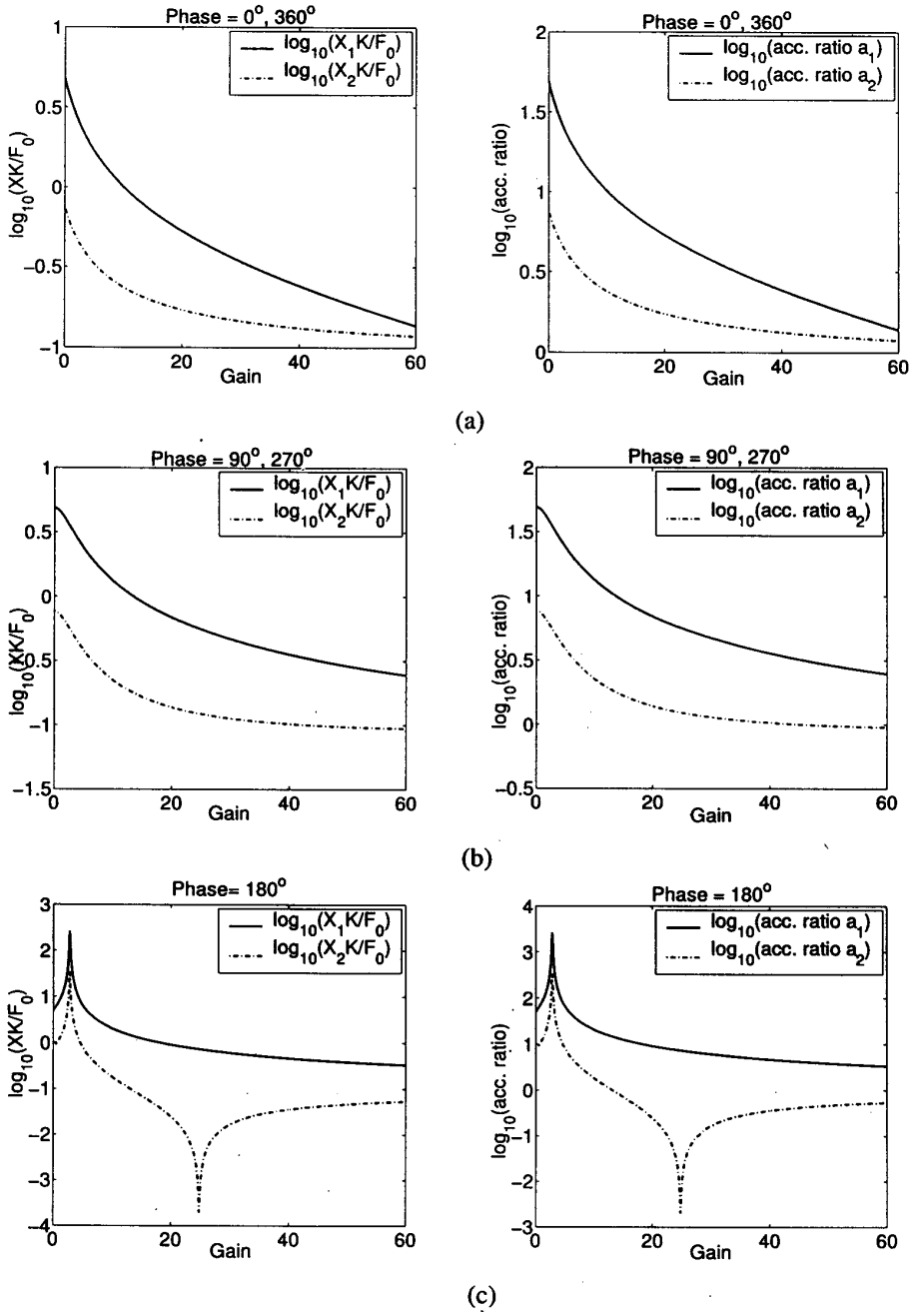

Fig.9 Influence of gain on the response of the closed loop vibration control system (excitation frequency of the system = 3.17 (21.5466 Hz)) (a) Phase = 0°,360°, (b) Phase = 90°, 270° and (c) Phase = 180°

show that as the mass is increased from 1.0 kg to 1.5kg, there is no significant shift in natural frequency of the system. From Fig.8a it can be noted that the non-dimensional natural frequency of the baseline system is 2.89. The non-dimensional natural frequency decreases to a value of 2.28 for an addition of absorber mass M_I = 1.0kg (Fig.13a); to 2.16 for absorber mass M_I = 1.3kg (Fig.13b); and to 2.09 for absorber mass M_I = 1.5kg (Fig.13c) respectively. The frequency response curves do not exhibit significant change in the characteristics, as is observed in the active control case (Fig.10). But, near the excitation frequency of 3.17, the acceleration response shows drastic

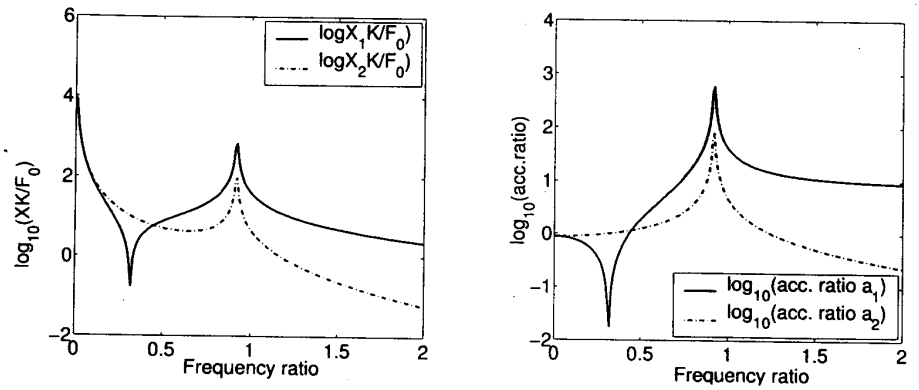

(a) $\bar{G} = 23$ and $\eta = 180^{\circ}$

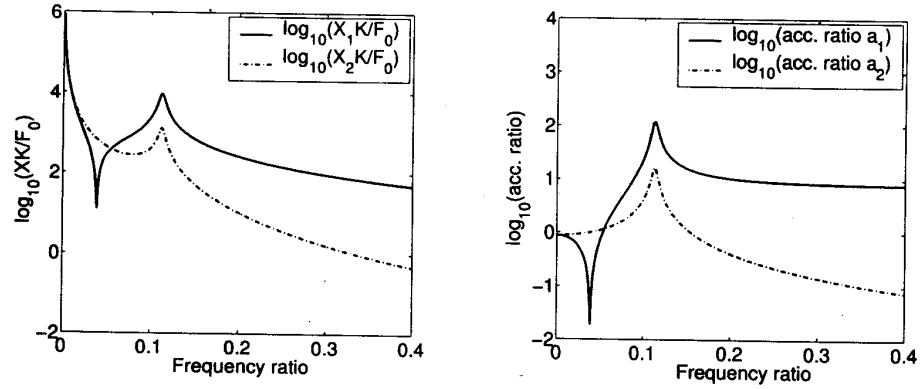

(b) $\bar{G} = 24.8$ and $\eta = 180^{\circ}$

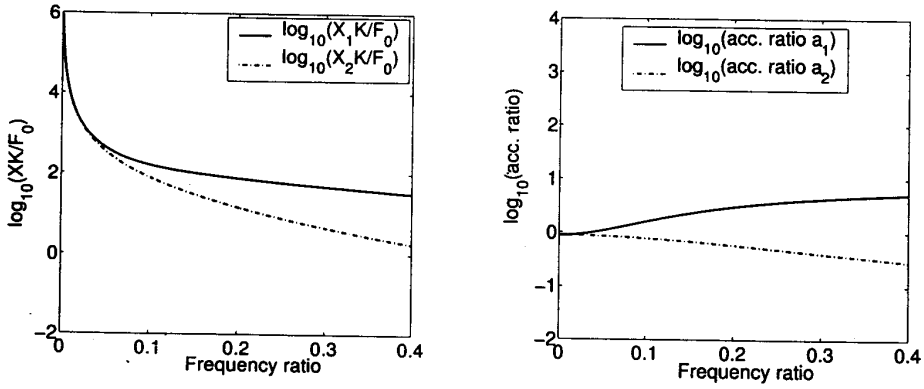

(c) $\bar{G} = 25$ and $\eta = 180^{\circ}$

Fig.10 Frequency response of closed loop system for different gain values
(a) $\overline{G}$ = 23 and η = 180°, (b) $\overline{G}$ = 24.8 and η = 180° and (c) $\overline{G}$ = 25 and η = 180°

change with respect to small variations in frequency (Fig.13). The asymptotic values of acceleration response of masses M_H and M_F, for absorber mass of M_I = 1.0 kg, 1.3 kg, and 1.5kg are 0.75, -0.58; 0.71, -0.49; and 0.68, -0.42 (Fig.13) respectively, which do not show significant variation contrary to what is observed in Fig.11.

Conclusions

This study presents the vibration control of a highly simplified two degree of freedom model of a helicopter. The vibration control study has been performed using the concept of ACSR for active vibration control and ARIS for passive vibration control. The reason for choosing

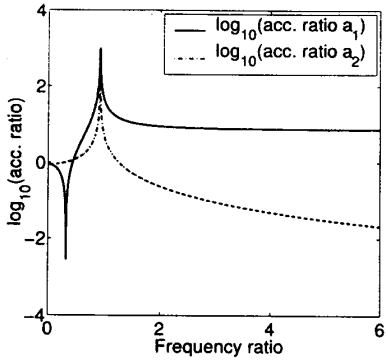

(a) $\bar{G} = 23$ and $\eta = 180^{o}$

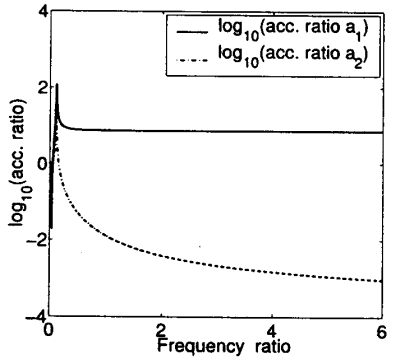

(b) $\bar{G} = 24.8$ and $\eta = 180^{o}$

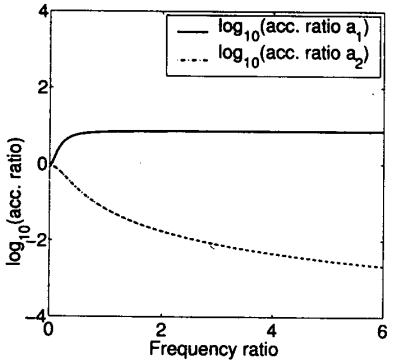

(c) $\bar{G} = 25$ and $\eta = 180^{o}$

Fig.11 Frequency response of closed loop system for different gain values (extended range)

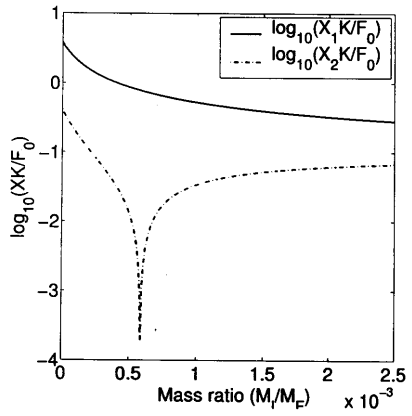

(a) Nondimensional displacement response

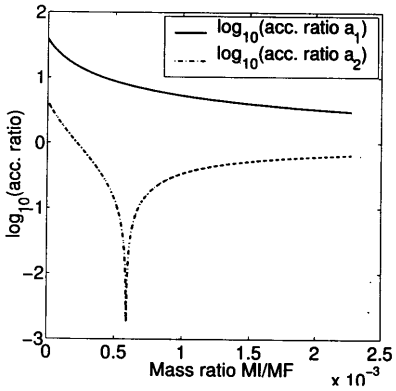

(b) Nondimensional acceleration response

Fig.12 Influence of absorber mass on response of passive system (excitation frequency of the system = 3.17 (21.5466 Hz))

these two schemes is that in both cases, the control force is proportional to the relative displacement between the hub and fuselage masses. In the case of active vibration control, the feedback mechanism affects the stiffness of the system; whereas in passive vibration control system, the absorber mass affects the inertia of the system. In the present study, the active control is achieved using piezo stack sensor and actuator mechanism. A finite element model for the piezo stack mechanism has been developed to obtain a relation between deformation, applied/induced potential and externally applied mechanical load. The important observations of vibration control study are as follows.

- In the case of active vibration control, inclusion of sensor and actuator units increases the natural frequency of the system due to increase in stiffness of the system. The results show that the there is sufficient gain and phase margin: available for closed loop vibration reduction. The minimum value of fuselage vibratory levels is obtained for a phase of 180deg.. Even though vibration reduction can be achieved for a wide range of values in gain and phase angles in the closed loop feedback system, the frequency response of the acceleration of the masses is observed to be highly sensitive to small variations in the magnitude of gain around the optimum value of gain. However, the effect of the

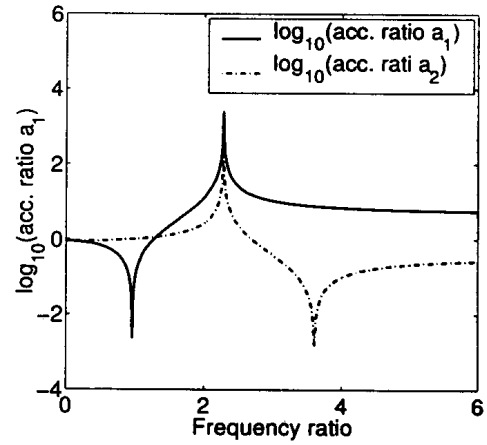

(a) $M_I = 1.0$kg

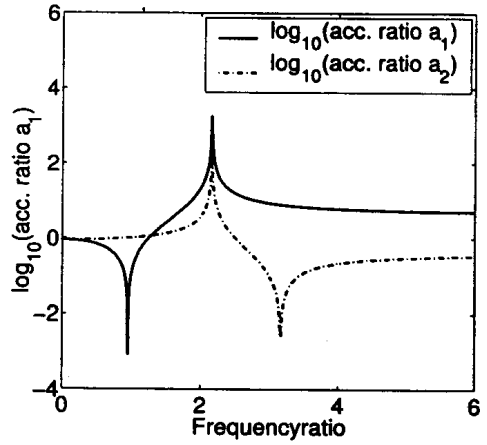

(b) $M_I = 1.3$kg

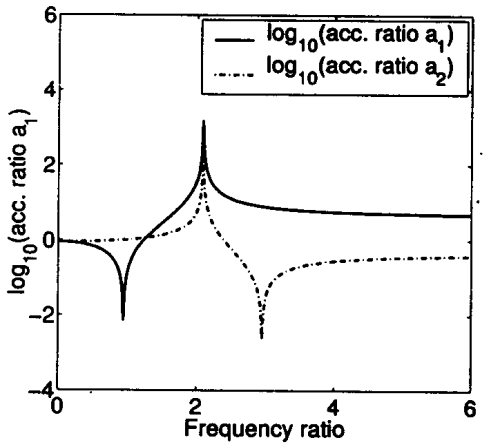

(c) $M_I = 1.5$kg

Fig.13 Influence of absorber mass on response of passive system (a) M_I = 1.0kg, (b) M_I = 1.3kg, and (c) M_I = 1.5kg

variation in frequency around the excitation frequency is found to be negligible on the response of the system.

- For the case of passive vibration control, the frequency response curves do not exhibit significant change in the characteristics with respect to variations in the absorber mass. However, the response is observed to be highly sensitive to small variation in the frequency around the excitation frequency.

- The results of present study indicate that closed loop feedback system for vibration reduction is better than the passive control system.

References

1. Kvaternik, R.G., Bartlett Jr. F.D. and Cline, J.H., "A Summary of Recent NASA/ARMY Contributions to Rotorcraft Vibrations and Structural Dynamics Technology", NASA/Army Rotorcraft Technology, CP - 2495, NASA, 1988, pp.71-179.

2. King, S.P. and Staple, A.E., "Minimization of Vibration Through Active Control of Structural Response", Rotorcraft Design Operations, CP-423, AGARD, 1986, pp.14.1-14.13.

3. Desjardins, R.A. and Euan Hooper, W., "Helicopter Rotor Vibration Isolation", Vertica, Vol.2, 1978, pp.145-159.

4. Braun, D., "Ground and Flight Tests of a Passive Rotor Isolation System for Helicopter Vibration Reduction", Vertica, Vol.8,1984, pp.1-14.

5. Sivaramakrishnan, R. and Venkatesan, C., "Rotor Fuselage Vibration Isolation Studies by a Floquet-Harrnonic Iteration Technique", Journal of Aircraft, Vol.27, No.1, January 1990, pp.81-89.

6. Rottmayr, H., Popp, W. and Mehlhose, R., "Application of Modern Vibration Control Techniques on EC135 and Future Trends", Proceedings of the 23rd European Rotorcraft Forum, Bonn, Sept. 1997, pp.51.1-51.17.

7. Welsh, W., Fredrickson, C., Rauch, C. and Lyndon, I., "Flight Tests of an Active Vibration Control System on the UH-60 Black Hawk Helicopter", Proceedings of the 51st Annual Forum of the American

Helicopter Society, American Helicopter Society, Alexandria, Virginia, USA, 1995, pp.393-402.

8. Anita Mathews, Sule, V.R. and Venkatesan, C., "Order Reduction and Closed-loop Vibration Control in Helicopter Fuselages", Journal of Guidance, Control, and Dynamics, Vol. 25, No.2, March-April 2002, pp.316-323.

9. Reichert, G. and Huber, H., "Active Control of Helicopter Vibration", Proceedings of the fourth workshop on Dynamics and Aeroelastic Stability Modeling of Rotorcraft Systems, Univ. of Maryland, College Park, USA, 1991, pp.1-20.

10. Cady, W.G., "Piezoelectricity - An Introduction to the Theory and Applications of Electro- Mechanical Phenomena in Crystals", First edition, Vols. I and II, Dover Publications Inc., New York, 1946.

11. Holland, R., "Design of Resonant Piezoelectric Devices", Research Monograph No.56, The M.I.T Press, Cambridge, Massachusetts, 1969.

12. Sheikh, N.A., Upadhyay, C.S. and Venkatesan, C., "Linear and Nonlinear Analysis of a Smart Beam using General Electrothermoelastic Formulation", AIAA Journal, Vol.42, No.4, April 2004, pp.840-849.

13. Sheikh, N.A., "Electro-Thermo-Elastic Formulation and Analysis of Smart Structures with Embedded Piezoelectric Material", Ph.D Thesis, Department of Aerospace Engineering, Indian Institute of Technology Kanpur, India, July 2003.

14. Reddy, J.N., "An Introduction to the Finite Element Methods, Second Edition, Tata McGraw Hill Publishing Company Limited, 1993, pp.67-141.